Effects on Conformational States of the Rabbit Sodium/Glucose Cotransporter through Modulation of Polarity and Charge at Glutamine 457

Tiemin Liu, Daniel Krofchick, and Mel Silverman*
Department of Medicine, University of Toronto, Toronto, Ontario, Canada

ABSTRACT   The high affinity sodium/glucose cotransporter (SGLT1) couples transport of Na^+ and glucose. Previous studies established that mutant Q457C human SGLT1 retains full activity, and sugar translocation is abolished in mutant Q457R or in mutant Q457C after reaction with methanethiosulfonate derivatives, but Na^+ and sugar binding remain intact. To explore the mechanism by which modulation of Q457 abolishes transport, Q457C and Q457R of rabbit SGLT1 were studied using chemical modification and the two-electrode voltage-clamp technique. Compared to wild-type SGLT1, Q457C exhibits ~20-fold reduction in phloridzin affinity and preferential occupancy of an inward-facing state. Alkylation of Q457C by [(2-trimethylammonium) ethyl] methanethiosulphonate bromide, (MTSET), reverses these changes while blocking transport. Analysis of pre-steady-state currents in the absence of sugar yields three decay constants for each of Q457C, Q457C-MTSET and Q457R. Comparison of Q457C-MTSET and Q457R with Q457C and wild-type, reveals that inhibition of transport is accompanied by a decrease in magnitude and voltage-independence of the slow decay constant at negative potentials. But fast and medium decays remain unchanged. Computer simulation of transient currents suggests that introduction of positive charge at position 457 leads to a predominant outward rather than inward-facing conformational state. Taken together, the results suggest that glutamine 457, in addition to being involved in sugar binding, is a residue that is sensitive to conformational changes of the carrier.

INTRODUCTION

The high affinity sodium/glucose cotransporter (SGLT1), responsible for intestinal glucose/galactose malabsorption, belongs to the homologous family of Na^+/solute symporters SLC5 (1). It is a secondary transporter that utilizes the sodium electrochemical gradient in a stoichometry of two Na^+ ions: one sugar molecule to transport sugar substrates against a concentration gradient. SGLT1 is expressed most abundantly at the mucosal surface of the small intestine and serves as the principal uptake pathway for glucose derived from dietary sources (2–4). The transporter is a monomer with 14 transmembrane domains. Investigation of the structure and function relationships of the SGLT1 is crucial to understanding cotransporter mechanism (5–10).

One polar residue at the carboxy-terminal part of transmembrane XI (Q457 of human SGLT1 (hSFLT1)) has been extensively investigated and proposed to be essential for the binding of sugar through hydrogen bond interactions with O1 and O5 of the pyranose ring (7,11–14). In addition, cysteine-scanning mutagenesis reveals that Q457R (a naturally occurring mutation in patients with glucose/galactose malabsorption) or Q457C reacting with thiol-reactive reagents (methanethiosulfonates and maleimides) abolishes sugar transport. However, under these conditions, it has been noted that the transporter still binds Na^+ and sugar (7, 15).

The objective of this study, therefore, was to better understand the role of glutamine 457 in affecting sugar transport. Mutants Q457C and Q457R of rabbit SGLT1 (rSGLT1) were expressed in the *Xenopus laevis* oocyte system and their functions were studied by the two-microelectrode voltage-clamp technique with a millisecond to second timescale. Glutamine to cysteine mutation at residue 457 in rSGLT1 causes ~20-fold reduction in phloridzin affinity and decreases the relative charge contribution of the charge due to depolarizing pulses (Q_{dep}) suggesting a predominant inward-facing state. However, alkylation of cysteine 457 through chemical modification by [2-(trimethylammonium) ethyl]methanethiosulfonate bromide;(MTSET) reverses the changes caused by this mutation at residue 457, while at the same time, blocking sugar transport. Analysis of pre-steady- state currents and computer simulation using a four state model shows that abolishing of sugar translocation correlates with an altered empty carrier transition state such that Q457C labeled MTSET (Q457C-MTSET) is predominant in the outward-facing state. The results of this study suggest that changes in polarity and charge at position 457 are associated with a minor modification of the orientation of the free carrier and a complete abolition of the translocation of the fully loaded carrier.

MATERIALS AND METHODS

Molecular biology

The mutants Q457C and Q457R were prepared by the site-directed mutagenesis using polymerase chain reaction protocol mutagenesis as described previously and confirmed by sequencing (6).

Oocyte preparation and injection

X. laevis were prepared as described previously (16). The oocytes were injected with 60 ng cDNA. The injected oocytes for the electrophysiology were stored at 16–18°C for four days or more.

Electrophysiology

Voltage clamping and recordings were performed using a GeneClamp 500 amplifier, Digidata 1200B interface, and pClamp 9.0 data acquisition software (Axon Instruments, Union City, CA) as described previously (17). The oocytes were constantly superfused with a solution for electrophysiological experiments consisting of 100 mM NaCl, 2 mM KCl, 1 mM MgCl$_2$, 1 mM CaCl$_2$, and 10 mM HEPES-Tris base (pH 7.4) and held at a holding potential, $V_{\rm h}$, of −50 mV, then was subjected to a series of voltage test pulses, test potential ($V_{\rm t}$). The current responses were recorded with a sampling interval of 20 μs for pre-steady-state and steady-state experiments. Results were filtered via a 1-kHz, 5-point Gaussian filter. Additional curve fitting was performed in ORIGIN 7.0 (OriginLab, Northampton, MA) with the Levenberg-Marquardt algorithm; n is the number of observations.

Transient current measurements

The rSGLT1 pre-steady-state currents were determined as described previously (6). The pre-steady-state currents for each $V_{\rm t}$ were integrated over the entire course of the trace to calculate the total charge transferred by the cotransporter. The charge, Q, was plotted as a function of the test pulses, and these Q ($V_{\rm t}$) curves were fitted to the two-state Boltzmann relation,

$$Q = -N \times e \times z \big(1 + exp(z \times u \times (V_{\rm t} - V_{0.5})) + Q_{\rm dep}\big), \qquad (1)$$

where Q is the total charge transferred, $Q_{\rm dep}$ is the charge due to depolarizing pulses, e is the elementary charge, z is the apparent valence of the movable charge, $V_{0.5}$ is the potential at which half of the total charge transfer is complete, and N is the number of cotransporters expressed at the surface. In the term $u = F/RT$; F is Faraday's constant, R is the gas constant, and T is absolute temperature.

Steady-state parameters were determined with the difference in the steady-state currents obtained before and after exposure to the substrate as described previously (6,18,19). Steady-state currents were acquired with test pulses of 300 ms duration. The final 100 ms of a test pulse were selected and the average current value of this range was acquired. The average current values were plotted versus substrate and the following equation was fitted to the curve,

$$I = I_{\rm max} \times [S]^n / ([S]^n + K_{0.5}^n), \qquad (2)$$

where S is the substrate of investigation (Na$^+$, α-methyl D-glucopyranoside (αMG)), $I_{\rm max}$ is the maximum current induced at saturating [substrate], n is the Hill coefficient, and $K_{0.5}$ is the Michaelis constant, which is the [S] at which the $I = I_{\rm max}/2$, which serves as an approximation of substrate affinity. The calculation of substrate affinity values used the $I_{\rm max}$ values of −150 mV test pulses.

Protocols for chemical modification

1 mM of cysteine-specific reagents, MTSEA, Na$^+$(2-sulfonatoethyl)methanethiosulfonate (MTSES), or MTSET (Toronto Research Chemicals, Toronto, Ontario, Canada), were dissolved in a voltage-clamping solution consisting of 100 mM NaCl, 2 mM KCl, 1 mM MgCl$_2$, 1 mM CaCl$_2$, and 10 mM HEPES-Tris base (pH 7.4) immediately before use. The oocytes expressing mutants were labeled with the bath solution including cysteine-specific reagents for 5–10 min, with membrane clamped at −50 mV.

Phloridzin affinity measurements

The phloridzin affinity was determined as described previously (20). Transient current measurements were made for an array of voltage steps ranging from −150 to 70 mV in 10 mV steps for mutants. The current recordings acquired in the presence of phloridzin (at the appropriate concentration) were subtracted from the recordings acquired in the absence of phloridzin

to obtain the phloridzin sensitive charge movement due to SGLT1. Subtracted data were then base line adjusted from 145–150 ms and integrated to give a Q/V distribution. The standard holding potential was −50 mV. At each membrane potential, charge versus phloridzin concentration was plotted and fitted to the Hill equation to find $K_{0.5}$.

State model simulations

State model simulations were performed as described previously (21). Transient currents of −130, −90, −10, 30, and 50 mV were simulated and fit simultaneously from 0 to 150 ms and from 150 to 300 ms. Eyring rate theory was used to calculate voltage dependence, V, of the rate constants. The overall χ^2 was minimized by optimizing 12 parameters: six rate constants (k) and six valences (z).

Statistical comparisons of means

Data are presented with mean $\pm$ SE. Comparisons of parameters were tested with t-test (ORIGIN 7). Statistical significance was accepted at an alpha level of $p < 0.05$.

RESULTS

Steady state kinetics of mutant Q457C of rSGLT1

The apparent affinity of mutant Q457C for sugar substrate αMG, ($K_{0.5}^{\alpha{\rm MG}}$), was determined by measuring αMG induced steady-state currents at various sugar concentrations and over a range of holding potentials. The results were then fitted according to the Michaelis-Menten equation. As shown in Fig. 1 A, the $K_{0.5}^{\alpha{\rm MG}}$ for mutant Q457C exhibits more voltage-dependence from −150 mV to −30 mV, compared to wild-type (WT) rSGLT1. The $K_{0.5}^{\alpha{\rm MG}}$ of mutant Q457C is 0.7 $\pm$ 0.1 mM ($V = -150$ mV) and 1.5 $\pm$ 0.2 mM ($V = -50$ mV); whereas for WT, $K_{0.5}^{\alpha{\rm MG}}$ is ~0.2 mM (from −150 mV to −50 mV).

To determine the Na$^+$ affinity of mutant Q457C, we measured αMG induced steady-state currents (obtained at saturating 20 mM αMG) at various Na$^+$ concentrations over a range of holding potentials and the resulting curves were analyzed using the Hill relationship (6). The Na$^+$ apparent $K_{0.5}$ of mutant Q457C exhibits relatively voltage-independent at hyperpolarizing membrane potentials from −150 mV to −80 mV and voltage-dependent from −70 mV to −30 mV (Fig. 1 B). The $K_{0.5}^{\rm Na^+}$ of mutant Q457C is 17.3 $\pm$ 2.6 mM ($V = -150$ mV) and 26.2 $\pm$ 3.2 mM ($V = -30$ mV). The corresponding values for n, the Hill coefficient range from 1.0 to 2.0. The $K_{0.5}^{\rm Na^+}$ of WT as previously determined is 8.3 $\pm$ 0.8 mM ($V = -150$ mV) and 41.9 $\pm$ 2.0 mM (V= −30 mV).

These results show that the glutamine to cysteine mutation at residue 457 in SGLT1 causes ~4-fold reduction in αMG affinity ($V = -150$ mV) and ~2-fold reduction in Na$^+$ affinity ($V = -150$ mV).

Pre-steady-state kinetics of mutants Q457C and Q457R of rSGLT1

Pre-steady-state currents for mutant Q457C were obtained as a function of voltage and integrated over 300 ms ($V_{\rm t}$) to
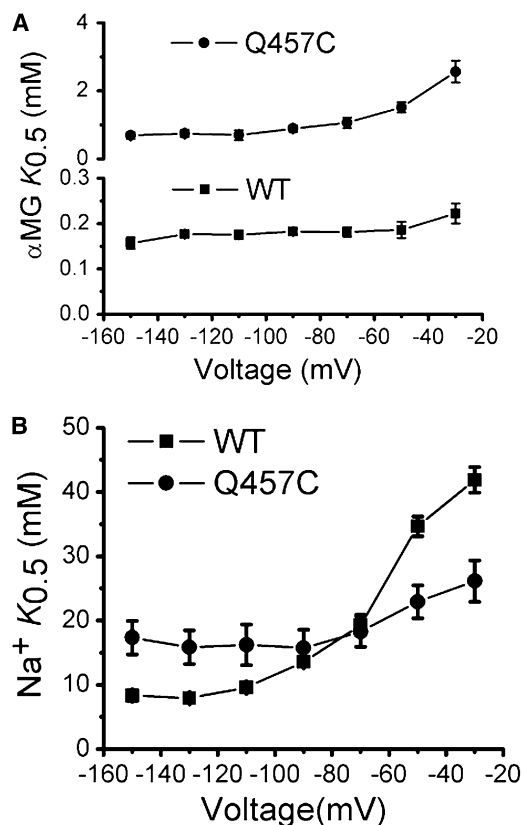
FIGURE 1 (A) αMG $K_{0.5}$ of WT rSGLT1 ($n = 3$) and Q457C rSGLT1 (n=3) for voltage dependence. The error bars represent SE. Q457C $K_{0.5}{}^{\alpha MG}$ was 0.7 ± 0.1 mM ($V = -150$ mV) and 1.5 ± 0.2 mM ($V = -50$ mV), representing significantly different values at -150 mV and -50 mV ($p < 0.05$). (B) The Na$^+$ $K_{0.5}$ of WT ($n = 3$) and Q457C ($n = 5$) for voltage dependence. The error bars represent SE. Q457C $K_{0.5}{}^{Na+}$ was 17.3 ± 2.6 mM ($V = -150$ mV) and 26.2 ± 3.2 mM ($V = -30$ mV), representing significantly different values at -150 mV and -30 mV ($p < 0.05$).

calculate total charge (Q) transferred by the cotransporter (V_h was -50 mV, V_t varied from -150 mV to $+70$ mV). The charge (Q) was then plotted as a function of the test pulses, and the $Q(V_t)$ curves were fit to the two-state Boltzmann equation. This protocol was carried out at 100 mM saturating Na$^+$ concentrations or 40 mM low Na$^+$ concentrations, and compared to WT rSGLT1.

In the presence of Na$^+$ and no sugar, the distribution of the cotransporter in outward-facing conformational states can be explained by the difference in the relative charge contribution of Q_{dep} (22). For WT rSGLT1 we have previously shown that in 40 mM Na$^+$ over the range -150 to $+70$ mV, there is ~80% charge recovery compared to 100 mM Na$^+$ (16), suggesting that WT SGLT1 exists primarily in outward-facing conformational states (substrate binding site exposed to the extracellular side) (22,23). In mutant Q457C, however, there is <50% charge recovery in the presence of 40 mM Na$^+$ compared that in 100 mM Na$^+$ (Fig. 2 A), suggesting preferential occupancy of the inward-facing state.

The mutation at residue 457 has altered voltage sensitivity (Table 1, Fig. 2 B). In 100 mM Na$^+$, the $V_{0.5}$ values of mutants Q457C and Q457R are shifted to negative potentials compared to WT (-20.0 ± 0.9 mV, -6.0 ± 5.2 mV, and -1.5 ± 5.1 mV, respectively).

Transporter turnover, k, was calculated using the empirical values for steady-state I_{max} and the pre-steady-state maximum charge transferred as calculated with the two-state Boltzmann relation (Q_{max}). The turnover of mutant Q457C and WT are 7.8 ± 0.9 s^{-1} ($n = 3$) and 9.8 ± 1.2 s^{-1} ($n = 4$), respectively. Therefore, the turnover rate for the mutant Q457C is decreased by ~20% compared to WT.

Chemical modification of mutant Q457C of rSGLT1 by methanethiosulfonate reagents

We next investigated the functional consequence of alkylation of cysteine 457 through chemical modification by methanethiosulfonate (MTS) reagents. Oocytes expressing mutant Q457C were exposed separately to positively charged MTS derivatives MTSET, MTSEA, and negatively charged MTSES, for 10 min in 100 mM Na$^+$, with the membrane clamped at -50 mV.

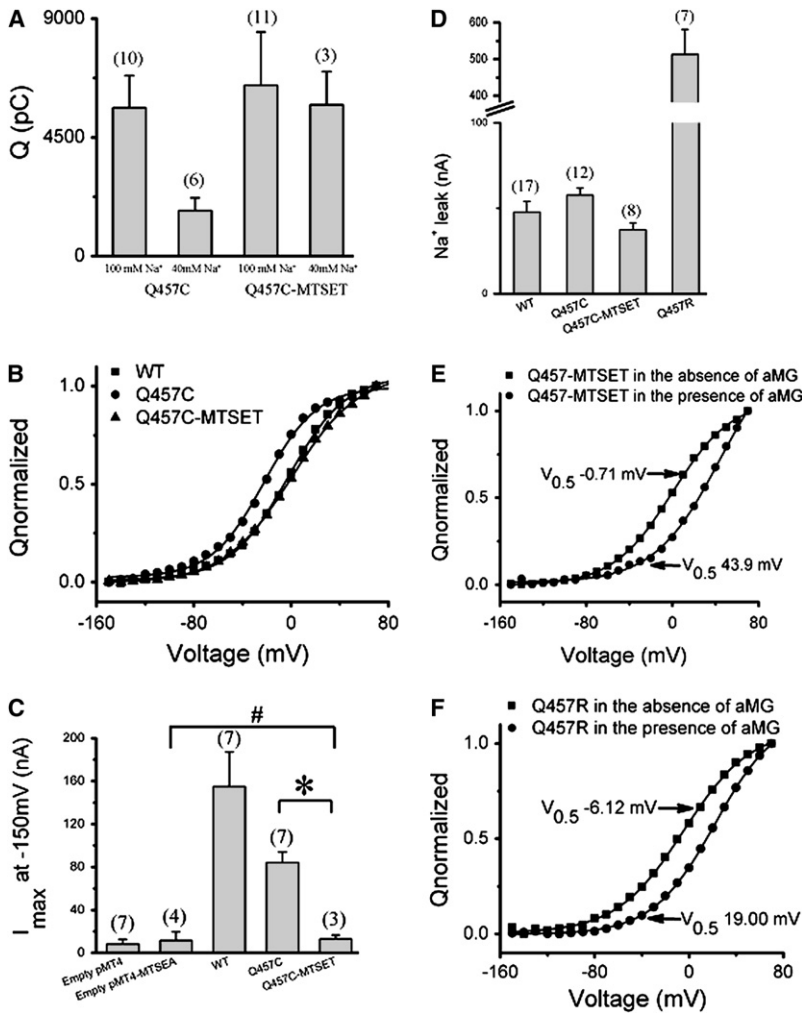### Effect of MTSET on voltage sensitivity and charge transfer of mutant Q457C

Fig. 2 shows the functional changes in Q457C after chemical modification by membrane-impermeant cationic MTSET. Representative normalized Q versus V curves obtained by integrating pre-steady-state currents in an oocyte expressing WT, mutant Q457C, mutant Q457C reacted with MTSET

TABLE 1   Pre-steady-state parameters for WT rSGLT1, mutant Q457C rSGLT1 before or after reaction with MTSET and mutant Q457R rSGLT1

	WT	Q457C		Q457C-MTSET		Q457R
	100 mM Na$^+$ ($n = 5$)	100 mM Na$^+$ ($n = 10$)	40 mM Na$^+$ ($n = 6$)	100 mM Na$^+$ ($n = 11$)	40 mM Na$^+$ ($n = 3$)	100 mM Na$^+$ ($n = 7$)
Q_{dep}/Q_{max} (%)	86	80	46	86	64	83
$V_{0.5}$ (mV)	-1.5 ± 5.1	-20.0 ± 0.9	-50.9 ± 1.0	-0.9 ± 0.5	-33.3 ± 0.5	-6.0 ± 5.2
dV (mV)	25.7 ± 2.5	20.7 ± 0.8	17.7 ± 0.9	28.0 ± 0.4	27.6 ± 0.5	27.3 ± 3.9
z	1.01	1.22	1.43	0.91	0.94	0.94

Pre-steady-state parameters were calculated by integrating the transient currents, and then fitted to a two-state Boltzmann relation.

FIGURE 2 (A) Comparison of the effects of 100 mM Na$^+$ and 40 mM Na$^+$ on charge transfer of mutant rabbit Q457C before and after exposure to MTSET ($n \geq 3$). The error bars represent SE. (B) Typical results demonstrating the effects on mutant Q457C charge transfer in oocytes treated with various 1 mM sulfhydryl-specific reagents (MTSET) in 100 mM Na$^+$. The $Q(V_t)$ curves were adjusted to zero at hyperpolarizing voltages (-150 mV) and normalized with respect to the extrapolated Q_{max}. (C) Comparison of the effects on maximum αMG-induced Na$^+$ currents measured at -150 mV in oocytes expressing of WT, or empty pMT4 plasmid before or after reaction with MTSEA, or mutant Q457C before or after reaction with MTSET ($n \geq 3$). The error bars represent SE. The "*" shows significant difference compared with I_{max} of mutant Q457C before or after reaction with MTSET at -150 mV ($p < 0.05$). The "#" shows no significant difference compared with I_{max} of empty pMT4 plasmid after reaction with MTSEA and mutant Q457C after reaction with MTSET at -150 mV ($p > 0.05$). (D) Comparison of the Na$^+$ leak currents measured at -150 mV in oocytes expressing of WT, or mutant Q457C before or after reaction with MTSET or mutant Q457R (n $\geq$ 3). The error bars represent SE. (E) The effect of sugar binding to mutant Q457C-MTSET on Q/V relations. The binding of sugar to mutant Q457C-MTSET can be studied from the effect of external sugar on the pre-steady-state charge movement. Sugar shifted the $V_{0.5}$ of the Q/V relation. Normalized Q/V curves at 0 and 20 mM αMG. The $V_{0.5}$ of the Q/V curve at 20 mM αMG shifted ~44 mV. (F) The effect of sugar binding to mutant Q457R on Q/V relations. Normalized Q/V curves at 0 and 10 mM αMG. The $V_{0.5}$ of the Q/V curve at 10 mM αMG shifted ~25 mV.

(Q457C-MTSET), or mutant Q457C reacted first with MTSET and then MTSEA. As shown in Fig. 2 B, after exposure to MTSET, the $V_{0.5}$ of Q457C is shifted toward more positive potentials ($V_{0.5} = -0.9 \pm 0.5$ mV, $n = 11$), so that the Q/V curve for Q457C-MTSET nearly superimposes on that of the WT. These results suggest chemical modification of Q457C by MTSET has reversed the changes in pre-steady-state behavior caused by the glutamine to cysteine mutation (see Methods and Materials section). These results are summarized in Table 1 where at 100 mM Na$^+$, the pre-steady-state parameters of WT and mutant Q457C-MTSET are almost equivalent. Furthermore, when mutant Q457C in the presence of Na$^+$ is sequentially reacted with MTSET, and then MTSEA, there is no additive effect on pre-steady-state behavior (data not shown).

We have previously shown that in 40 mM Na$^+$ there is ~80% charge recovery for WT and ~50% charge recovery for mutant Q457C compared to 100 mM Na$^+$. Alkylation of Q457C by MTSET substantially reverses the effect caused by the glutamine to cysteine mutation. The Q/V of mutant Q457C-MTSET in 40 mM Na$^+$ represents ~80% of the

charge transferred in 100 mM Na$^+$ (Fig. 2 A), suggesting an increase in occupancy of the outward-facing state.

Effects of MTSET on sugar transport and sugar binding of mutant Q457C

As observed previously for mutant Q457C hSGLT1 (7), alkylation of cysteine 457 in mutant Q457C rSGLT1 after exposure to MTSET results in inhibition of steady-state αMG induced Na$^+$ currents (Fig. 2 C).

Fig. 2 D shows that the Na$^+$ leak of Q457C-MTSET is also reduced (~65% of mutant Q457C). The Na$^+$ leak values of WT, mutants Q457C, Q457C-MTSET and Q457R for rSGLT1 are -47.8 ± 6.3 nA ($n = 17$), -57.6 ± 4.1 nA ($n = 12$), -37.4 ± 4.1 nA ($n = 8$) and -513 ± 68 nA ($n = 7$), respectively. Similarly, previous studies have shown that alkylation of mutant Q457C with MTSEA (Q457C-MTSEA) for hSGLT also had relatively large Na$^+$ leak (Q457C and Q457C-MTSEA are ~131 nA and ~314 nA, respectively) (7).

The effect of the external αMG on pre-steady-state charge movement can be used to study sugar-binding characteristics

of mutants Q457C-MTSET and Q457R. As described by Gagnon et al. (23), transporter specific pre-steady-state currents were obtained by subtracting currents in the presence of 200 μM phloridzin from currents measured in the absence or presence of αMG. Although alkylation of Q457C by MTSET inhibits sugar transport, Fig. 2 E reveals that addition of 20 mM αMG causes the $V_{0.5}$ of mutant Q457C-MTSET to shift ~44 mV along the voltage axis. This result indicates that sugar binding of mutant Q457C-MTSET is still present. Fig. 2 F reveals that an addition of 10 mM αMG causes the $V_{0.5}$ of mutant Q457R to shift ~25 mV along the voltage axis and also suggests that sugar binding of mutant Q457R is still present.

These results obtained for mutants Q457C-MTSET and Q457R rSGLT1 are consistent with those reported for mutants Q457C-MTSET and Q457R from hSGLT1 (7,15).

Effect of MTSES or MTSEA on mutant Q457C

MTSES altered pre-steady-state currents such that at both depolarizing (+70 mV) and hyperpolarizing (−150 mV) potentials there was no saturation of charge transfer and it was not possible to obtain a fit of the data to a two-state Boltzmann relation. MTSEA caused a marked increase in Na^+ leak substantially reducing the observable charge transfer associated with cotransporter activity (data not shown). As a consequence of these findings, the effects of chemical modification by MTSES and MTSEA were not further analyzed.

Phloridzin affinity

The specific inhibitor, phloridzin, binds to SGLT1 and blocks sugar translocation (24). As described in the Materials and Methods section, the ability of phloridzin to reduce transient charge movement of SGLT1 can been used to measure its apparent affinity for the cotransporter (20,23–25). As shown in Fig. 3, the phloridzin substrate concentration at 0.5 I_{max} ($K_{0.5}$) of Q457C is 30.7 ± 0.7 μM, indicating that the glutamine to cysteine mutation at 457 has reduced phloridzin affinity by ~20-fold, compared to WT (1.4 ± 0.2 μM, data not shown). When a positive charge is introduced at position 457 by reacting cysteine 457 with MTSET, however, the phloridzin $K_{0.5}$ of mutant Q457C is 4.5 ± 0.1 μM, indicating that alkylation with MTSET (Q457C-MTSET) has rescued the phloridzin affinity of mutant Q457C (which is now reduced by ~3-fold, compared to WT).

Decay constants of Q457C of rSGLT1

A simple six-state model has been used to explain the kinetics of SGLT1 function in a limited time range (Fig. 4 A) (7). States C_1 and C_6, C_2 and C_5, and C_3 and C_4 represent the empty [C], Na^+-bound [CNa_2], and Na^+- and sugar-bound conformations [$SCNa_2$] of the cotransporter at the external and internal membrane surfaces.
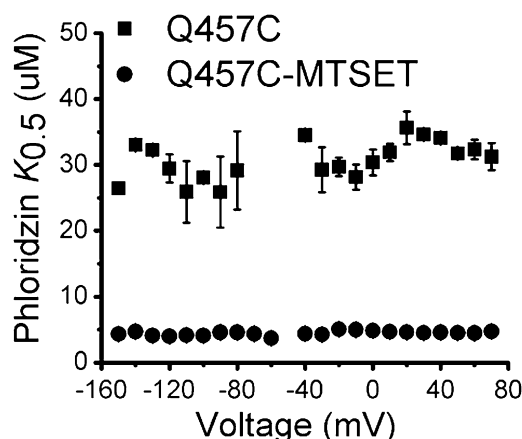

FIGURE 3   Estimation of the phloridzin $K_{0.5}$ of rabbit Q457C and Q457C-MTSET for voltage dependence with the transferred charge ($n \geq 3$). Voltage dependent transferred charge in the presence of various concentrations of phloridzin was fitted to the Hill relationship. The error bars represent SE.

The pre-steady-state currents in an oocyte expressing SGLT1 consist of a nonspecific component (due to oocyte membrane capacitance) and an SGLT1 specific component. To isolate SGLT1 specific currents, the well-known non-transported sugar inhibitor, phloridzin, is used to block SGLT1 activity. Then, recorded currents acquired in the presence of saturating phloridzin (200 μM) are subtracted from currents acquired in the absence of phloridzin, to provide the currents due exclusively to SGLT1.

In the presence of Na^+ and absence of sugar, using the two-electrode voltage clamp technique and the phloridzin subtraction protocol with sufficient duration of voltage pulse (150 ms), there is now evidence or an additional intermediate empty carrier conformational state (C_{1a}) (Fig. 4, B and C) (21,26). Thus, it is now believed that reorientation of empty carrier from an inward to outward-facing state occurs via two transitions, $C_6 \leftrightarrow C_{1a}$, $C_{1a} \leftrightarrow C_1$. The cotransporter is in state C_2 at large hyperpolarizing voltages, and at C_6 at large depolarizing voltages. In the presence of Na^+ and absence of sugar, the four transporter transition states are characterized by three time constants (21).

Accordingly, the pre-steady-state transient currents of mutants Q457C and Q457C-MTSET were fitted to obtain first-, second-, and third-order decays. Fig. 5 shows the fit to the pre-steady-state currents for mutants Q457C (Fig. 5, A and B) and Q457C-MTSET (Fig. 5, D and E), using first- and second- order exponential decays. The nonrandom regions in the first 25 ms (Fig. 5, B and E) demonstrate inadequacy of the fit with second- order exponential decays. The residuals of the third-order exponential decay (Fig. 5, C and F) exhibit random oscillations about the zero axis, indicating best fit of the data with three exponential decay components for the pre-steady-state currents of mutants Q457C and Q457C-MTSET. These results suggest that the pre-steady-state currents of mutants Q457C and Q457C-MTSET can also be represented by three decay constants (τ_f, the fast
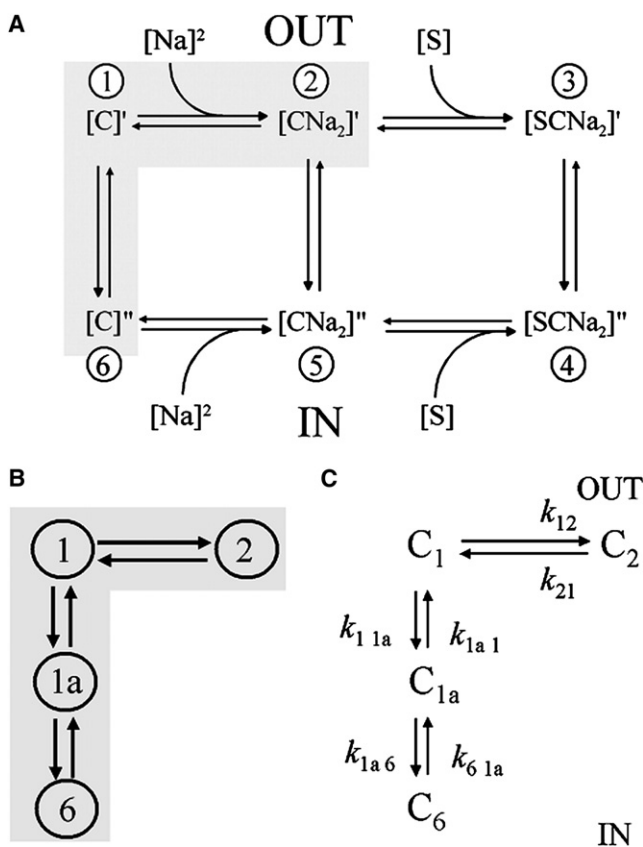
FIGURE 4   Kinetic models for SGLT1 in the presence of sugar or absence of sugar. (*A*) A simple six-state model for SGLT1 with sugar in a certain time range (7). The shaded region represents the voltage-dependent step: Na^+ binding/dissociation $C_2 \leftrightarrow C_1$; orientation of empty carrier between inward-facing state and outward-facing state $C_1 \leftrightarrow C_6$. (*B*) A four-state model of SGLT1 for pre-steady-state currents in the absence of sugar (21,26), which added an intermediate empty carrier conformational state (C_{1a}) between C_1 and C_6. (*C*) In the absence of sugar, a four-state model of SGLT1 for charge movement, decay constants (τ) and rate constants (k).

FIGURE 5   Fit residuals for mutant rabbit Q457C before or after reaction with MTSET. First- (*A*) or (*D*), second- (*B*) or (*E*), and third- (*C*) or (*F*) order fit residuals for the -130 mV prestep, 10 mV poststep potential transient.

decay constant; τ_m, the medium decay constant; and τ_s, the slow decay constant), consistent with those reported for WT rSGLT1 (21).

Fig. 6, *A–C*, show the relationships between decay constants and voltage. Inspection of Fig. 6 reveals that in the presence of 100 mM Na^+, the three decay constants for WT (21) and mutant Q457C are similar both in magnitude and voltage dependence. The fast decay constant of mutant Q457C (τ_f, 0.5–1.1 ms) is relatively voltage-independent with a range between 0.5 ms and 1.1 ms (Fig. 6 *A*). The medium decay constant of mutant Q457C (τ_m, 1.2–6.5 ms) has a voltage-dependence and increases from ~1.2 ms at hyperpolarizing potentials to ~6.5 ms at depolarizing potentials (Fig. 6 *B*). The slow decay constant of mutant Q457C (τ_s, 60–15 ms) has a sigmoid-shaped voltage-dependence and decreases rapidly from ~60 ms at hyperpolarizing potentials to ~15 ms at depolarizing potentials (Fig. 6 *C*).

At low Na^+ concentrations (40 mM Na^+), both the fast decay constant (τ_f, 0.9–1.3 ms) and the medium decay
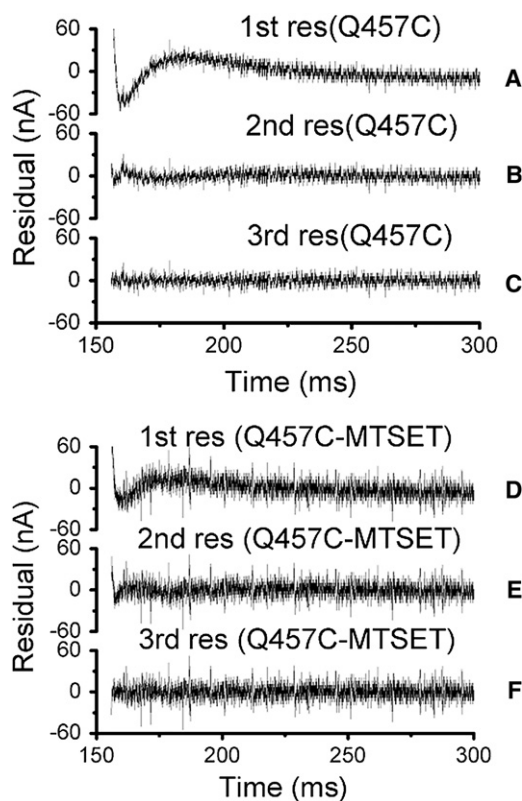
constant (τ_m, 1.4–5 ms) are only slightly altered (Fig. 6, *A* and *B*). But the slow decay constant (τ_s, 100–6.5 ms) is significantly slower at potentials more hyperpolarizing than -50 mV and faster at potentials more depolarizing than -50 mV (Fig. 6 *C*).

The decay constants for mutants Q457C-MTSET and Q457R are illustrated in Fig. 6, *D–F*. In the presence of 100 mM Na^+, the fast decay constant (τ_f, 0.5–1.4 ms) and the medium decay constant (τ_m, 1.2–6 ms) for both Q457C-MTSET and Q457R are similar to that of WT and mutant Q457C (Fig. 6, *D* and *E*). However, the slow decay constant (τ_s) of Q457C-MTSET and Q457R are substantially changed. Both exhibit voltage-independence from -150 mV to 0 mV, with reduced magnitudes of ~30 ms and ~16 ms, respectively. At depolarizing voltages (≥ 20 mV), the slow component exhibits very low amplitude of the transient currents (small signal/noise ratio), precluding our obtaining estimates of τ_s for mutants Q457C-MTSET and Q457R over this voltage range.

The slow decay constants of mutants Q475C-MTSET and Q457R are reduced in magnitude (i.e., faster) at potentials more hyperpolarizing than -50 mV and increased in magnitude (i.e., slower), at potentials more depolarizing than -50 mV, compared to the slow decay constant of mutant Q475C (compare Fig. 6 *C* and *E*). When the Na^+ concentration
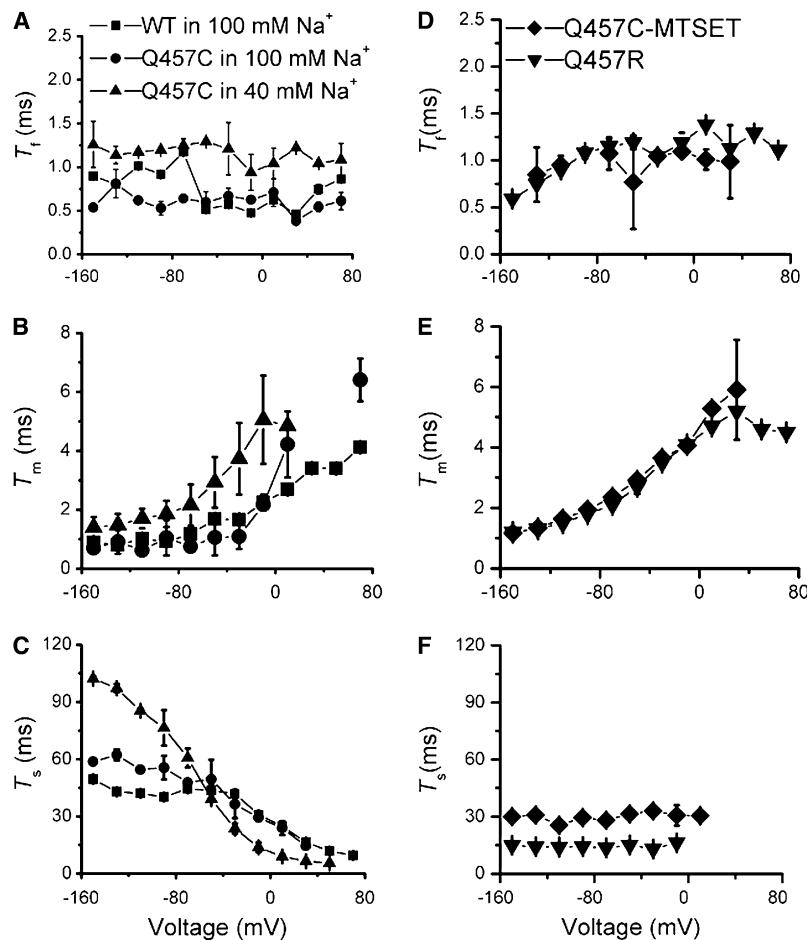
FIGURE 6 Voltage- and Na$^+$-dependence of the three decay constants ($n \geq 3$). For WT in 100 mM Na$^+$ (■) and mutant Q457C in 100mM (●) and 40 mM Na$^+$ (▲) (A) τ_f, fast decay. (B) τ_m, medium decay. (C) τ_s, slow decay. For mutants Q457C-MTSET in 100 mM Na$^+$ (◆) and Q457R in 100 mM Na$^+$ (▼), (D) τ_f, fast decay. (E) τ_m, medium decay. (F) τ_s, slow decay.

is reduced from 100 mM to 40 mM, a condition in which Q457C exists preferentially in an inward facing conformational state, we observe a marked slowing of τ_s compared to mutants Q475C-MTSET and Q457R (Fig. 6 C). Collectively, these results suggest that addition of positive charge at position 457 significantly increases return of empty carrier from inward-facing state to outward-facing state.

Table 2 summarizes the decay constants (τ) for WT in 100 mM Na$^+$, mutants Q457C in 100 and 40 mM Na$^+$, Q457C-MTSET in 100 mM Na$^+$ and Q457R in 100 mM Na$^+$.

Model simulations

Computer model simulations were carried out based on a four-state model (Fig. 4 B) proposed by Chen et al. (26)

and Krofchick et al. (21), to help evaluate the functional differences between WT and mutant Q457C before and after reaction with MTSET. The top panels of Fig. 7, A and B show the simulated pre-steady-state currents and charge transfer using the best-fit parameters in Table 3. The bottom panels of Fig. 7, A and B show the three decay constants plotted as a function of voltage and compared to the experimentally derived τ values in Fig. 6. As shown in the middle panels of Fig. 7, A and B, the ON and OFF charges in the experiments are not equal. Although the reason for this phenomenon is unknown, similar results have been shown by Loo et al. (27). One possibility is that these currents do not represent pure displacement currents (i.e., currents due to the displacement of charged residues attached to the transporter). Fig. 7 reveals good agreement between model

TABLE 2 Summary of the time constants for WT and mutants

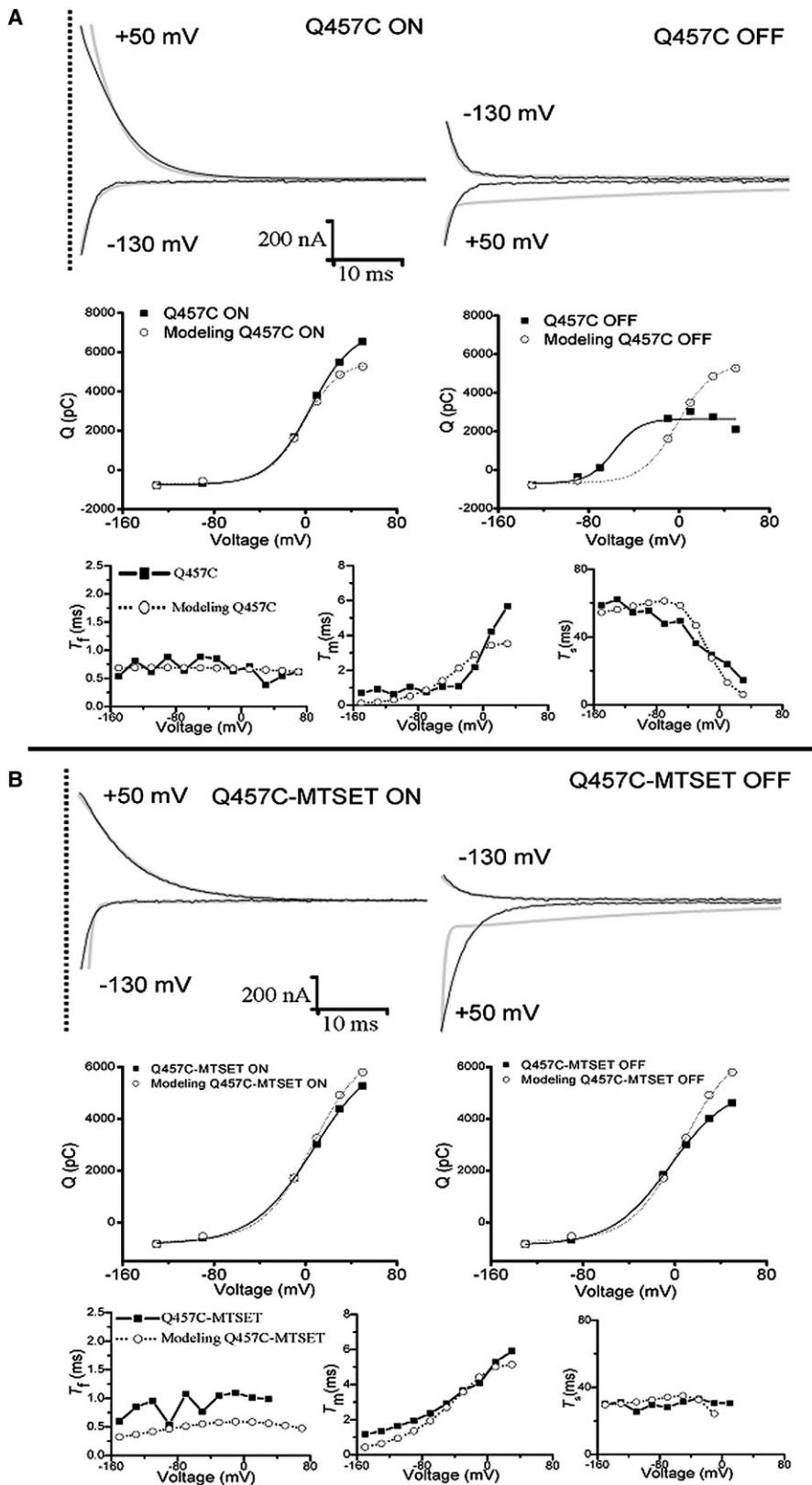|	[Na$^+$] (mM)	The fast decay constant (τ_f)	The medium decay constant (τ_m)	The slow decay constant (τ_s)
rWT	100	0.5–1 ms	0.5–4 ms	50–8 ms
rQ457C	100	0.5–1 ms	1.2–6.5 ms	60–15 ms
	40	0.9–1.3 ms	1.4–5 ms	100–6.5 ms
rQ457C-MTSET	100	0.5–1.1 ms	1.2–6 ms	~30 ms
rQ457R	100	0.5–1.4 ms	1.2–6 ms	~16 ms

FIGURE 7 Simulated transient currents, charge transfer and decay constants in 100 mM Na$^+$ were predicted by the model solution in Table 3. Predictions of the kinetic model superimposed on the experimental data for mutant Q457C rSGLT1 (*A*) and mutant Q457C exposed to MTSET rSGLT1 (*B*). The top panel shows simulated currents (*gray line*) at the potentials of -130 mV and $+50$ mV superimposed on the experimental current (*black line*). The middle panel illustrates the *Q/V* curves. The bottom panel shows three decay constants (τ_f, the fast decay constant; τ_m, the medium decay constant; and τ_s, the slow decay constant) as a function of voltage.

simulations and experimental data for mutants Q457C and Q457C-MTSET for pre-steady-state ON currents, the medium decay constant, and the slow decay constants. In contrast, Fig. 7 reveals a difference between model simulations and experimental data for pre-steady-state OFF currents and the fast decay constants. The model proposed with the

TABLE 3 Rate constants of a four-state kinetic model used for the pre-steady-state current simulations of WT rSGLT1 and mutants in 100 mM Na$^+$

		(s^{-1})													
	k_{21}	k_{12}	$k_{1\ 1a}$	$k_{1a\ 1}$	$k_{1a\ 6}$	$k_{6\ 1a}$	Z_{21}	Z_{12}	$Z_{1\ 1a}$	$Z_{1a\ 1}$	$Z_{1a\ 6}$	$Z_{6\ 1a}$	k_{21}/k_{12}	$k_{1\ 1a}/k_{1a\ 1}$	$k_{1a\ 6}/k_{6\ 1a}$
WT (21)	66	180	100	24	330	380	0.44	0.69	0	0	0.31	0.2	0.37	4.2	0.87
Q457C	150	160	80	24	750	850	0.3	0.7	0.8	0	0.17	0.07	0.94	3.3	0.88
Q457C-MTSET	90	120	80	36	750	850	0.3	0.5	0.8	0	0.25	0.2	0.75	2.2	0.88

parameters shown in Table 3 represents fairly well the ON data for mutants Q457C and Q457C-MTSET. The reason for the poor fit to the OFF data is unknown but it clearly indicates that the real mechanism responsible for the transient current recorded is more complex than the proposed model.

A summary of representative model parameters for mutants Q475C and Q475C-MTSET derived from model simulations is shown in Table 3. Comparing the parameter values for WT and mutant Q457C (Table 3), the ratio for transitions $C_{1a} \leftrightarrow C_6$ are similar. But the ratio for transition $C_2 \leftrightarrow C_1$, the Na$^+$ dissociation rate k_{21} / k_{12}, is altered (0.37 for WT versus 0.94 for mutant Q457C), which correlates with the observed decrease in $K_{0.5}^{Na^+}$ of Q457C. Reacting mutant Q457C with positively charged MTSET, partly restores the Na$^+$ dissociation rate k_{21} / k_{12} (0.75 for Q457C-MTSET versus 0.94 for Q457C). Computer simulation also reveals that the rate observed for empty carrier transition from outside to inside, $k_{1\ 1a}/k_{1a\ 1}$, decreases from 4.2 for WT to 2.2 for mutant Q457C-MTSET. This suggests that there is a faster rate for reorientation of empty carrier back to the outside facing state and correlates with the increase in Q_{dep}/Q_{max} for the inward/outward-facing distribution and abolishing of sugar translocation.

DISCUSSION

In hSGLT1, mutant Q457R or mutant Q457C exposed to thiol-reactive reagents (methanethiosulfonates and maleimides), abolishes sugar translocation. However, under these conditions, the transporter still binds Na$^+$ and sugar (7). The sugar (αMG) affinities of mutants Q457E (polar to negative) (13), Q457C (polar to neutral) (13) and Q457R (polar to positive) (1,15) are reduced by ~4, ~7, and ~10-fold respectively, compared to WT, suggesting that the position 457 is quite tolerant to charge. Diez-Sampedro et al. (13) compared the kinetics of transport of glucose analogs (each modified at one position of the pyranose ring) for hSGLT1, Q457C and Q457E and then proposed that Q457 was essential for binding of sugar through hydrogen bond interactions with O1 and O5 of the pyranose ring.

Because Q457 hSGLT1 is tolerant to charge and still binds to sugar in the absence of transport, it seemed to us that Q457 is more important for translocation of sugar. To further investigate this issue, mutants Q457C and Q457R in rSGLT1 were characterized using the two-electrode voltage-clamp technique. Our experimental findings indicate similar functions of rabbit and human isoforms after a glutamine to cysteine mutation (Q457C) with regard to decreased apparent affinity for αMG and Na$^+$. Also in both instances of Q457R or Q457C reaction with MTSET abolishes sugar transport, leaving binding of Na$^+$ and sugar intact.

But the results of our study also provide what we believe are new insights into the functional significance of glutamine 457 in rSGLT1. Specifically our findings support the hypothesis that loss of sugar transport in the mutants Q457C-MTSET and Q457R of rSGLT1, can be explained by changes in the conformational equilibrium of the transport cycle with accumulation of transporter in an outward-facing state. The evidence supporting this hypothesis is discussed below.

Our data shows that most of the transporters remain in a nontransporting outward-facing state as a consequence of reacting Q457C rSGLT1 with MTSET. Therefore, the cotransporter under these conditions is more available for binding of phloridzin, and the substantial alteration in phloridzin affinities of mutants Q457C and Q457C-MTSET (Fig. 3) can be explained on the basis of a changed equilibrium between inward- and outward-facing conformational states. Changes in the equilibrium between inward- and outward-facing conformational states and altered substrate/inhibitor affinity have been observed for other transporters. For example, mutant D176A rSGLT1 exhibits an increased rate of empty carrier transition from outside to inside, which is accompanied by a decreased apparent affinity for phloridzin (28). Mutants K264A, Y335A and D345A alter the conformation of the dopamine transporter and result in changed apparent affinities for inhibitors (29). Mutant M345H in the γ-aminobutyric acid transporter-1 (that belongs to a large family of Na$^+$/Cl$^-$-coupled neurotransmitter transporters) shifts the transporter toward the outward-facing Na$^+$-bound conformation, resulting in an increased apparent affinity for Na$^+$ (30). Finally, mutant T349H in the γ-aminobutyric acid transporter-1 shifts the transporter toward the inward-facing empty conformation causing a decrease in the apparent affinity for Na$^+$ (30).

A common behavior observed for ion-coupled cotransporters is that the empty carrier will orientate from internal to external membrane surface during the initial transport step and is associated with charge movement (11,31,32). For example, Loo et al. (7,11,12) studied the fluorescence changes of tetramethylrhodamine-6-maleimide-labeled
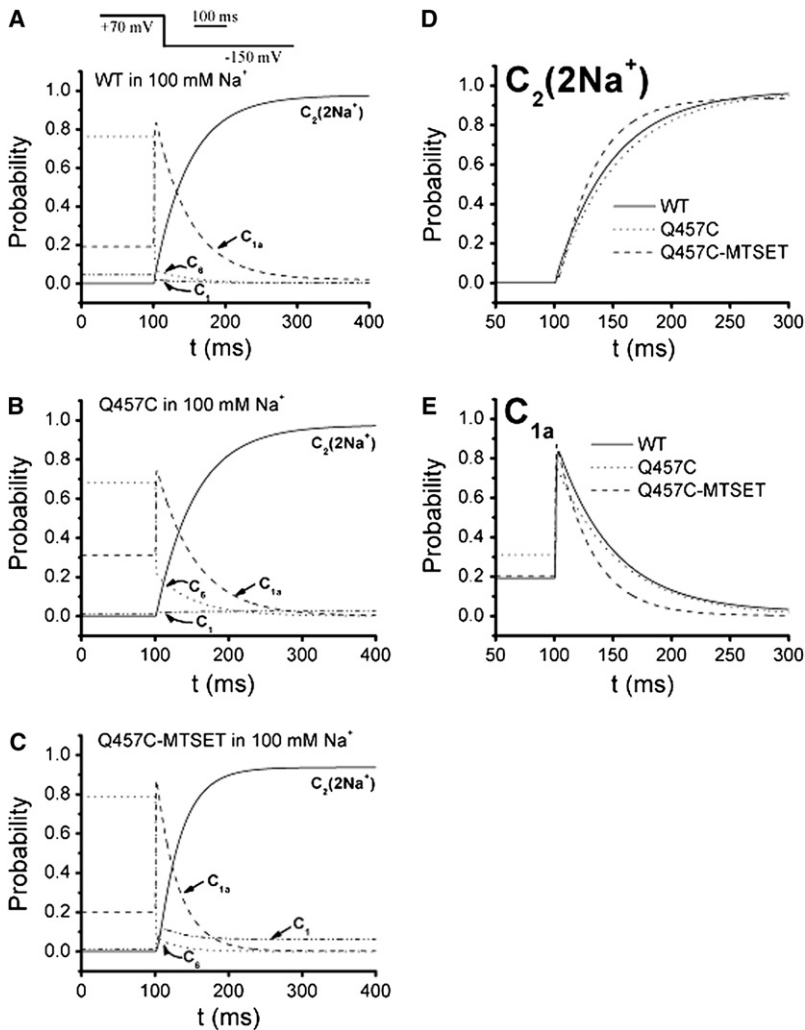
FIGURE 8   Occupancy probability (C_i) in 100 mM Na^+ as a function of time as calculated by the four-state kinetic model for WT r SGLT1 and mutant Q457C before or after exposed to MTSET. (*A*) Time course of WT occupancy probabilities for a V_m pulse from +70 mV to −150 mV. (*B*) Time course of mutant Q457C occupancy probabilities for a V_m pulse from +70 mV to −150 mV. (*C*) Time course of mutant Q457C exposed to MTSET occupancy probabilities for a V_m pulse from +70 mV to −150 mV. (*D*) Time course of WT (*solid line*), Q457C (*dotted line*), and Q457C-MTSET (*dashed line*) C_2 occupancy probability for a V_m pulse from +70 mV to −150 mV. (*E*) Time course of WT (*solid line*), Q457C (*dotted line*), and Q457C-MTSET (*dashed line*) C_{1a} occupancy probability for a V_m pulse from +70 mV to −150 mV.

human Q457C (Q457C- tetramethylrhodamine-6-rhodaminemaleimide (TMR6M)) under voltage clamp, and suggested the major voltage-dependent step in the SGLT1 transport cycle was the return of the empty carrier from inward-facing to outward-facing states. Also, based on a four-state model for SGLT1, charge movements were associated with conformational transitions of sodium binding/debinding ($C_1 \leftrightarrow C_2$) and reorientation of the unloaded protein across the membrane ($C_1 \leftrightarrow C_{1a} \leftrightarrow C_6$) (Fig. 4, *B* and *C*) (21).

Thus, SGLT1 pre-steady-state currents provide direct insight into the conformational changes that accompany rearrangements of charges within the protein. In particular, the slow decay constant reflects the rate limiting transition of the empty carrier (9). However there is some discrepancy in the results for Q457C reacted with MTS and maleimides from earlier investigations. Previous studies recording charge movement reported that the slow decays (τ_s) of mutant Q457C-TMR6M hSGLT1 (11) is voltage-dependent and Na^+-dependent, whereas the results from recording fluorescence changes seems to indicate that the slow decay (τ_s) of mutant Q457C-TMR6M hSGLT1 is voltage-dependent

and Na^+- independent. These differences may be due to the different experimental protocols used and the very low amplitude of the transient currents exhibited by the slow component (small signal/noise ratio). The pre-steady- state currents for slow component of mutant Q457C-TMR6M hSGLT1 was <20 nA between −150 mV and +50 mV, compared to ~200 nA for total components of mutant Q457C-TMR6M hSGLT1 (11). The fluorescence level for the controls, TMR6M-labeled hSGLT1 Q457C expressing oocytes was 187 ± 15 au and 229 ± 25 au, respectively (12). The ΔF for slow component of mutant Q457C-TMR6M hSGLT1 was 0.36 au at −190 mV and 0.38 au at +90 mV (11).

In this study, to resolve the experimental difficulty of dealing with small signals for the slow component, we took advantage of the modified OFF protocol (21) that yields adequate currents at large voltage jumps, to obtain estimates of τ_s for mutants Q457C-MTSET and Q457R of rSGLT1. Our experimental data and the computer simulations based on a four-state model lend further support to the conclusion that addition of a positive charge at position 457 significantly

slows the return of the empty carrier from an outward-facing to inward-facing state. It is interesting that similar results have been found for three other SGLT1 mutants:Q170E rSGLT1 (22), C255A hSGLT1 (23) and C511A hSGLT1 (23). In each case, the major changes identified in the computer simulations are that the rate of the empty carrier from outside to inside ($k_{1\ 1a}$ / $k_{1a\ 1}$) is decreased, resulting in a greater number of transporters in the outward-facing state (22,23,33).

The occupancy probability (C_i) as a function of time as calculated by kinetic model for SGLT1 has been used to evaluate the functional differences between WT and mutants (23,24,34) of rSGLT1. Based on a four-state model (Fig. 4 B), the computer model simulations for occupancy probability (C_i) as a function of time as calculated by the four-state kinetic model for WT rSGLT1 and mutant Q457C before or after exposure to MTSET in the presence of 100 mM Na$^+$ and absence of αMG, could help us to evaluate the functional differences between WT and mutant Q457C before and after exposure to MTSET. Fig. 8 shows the occupancy probabilities for a voltage step from the most depolarizing potential (+70 mV; most of the transporters will stay in the inward-facing states) to the most hyperpolarizing potential (−150 mV; most of the transporters will stay in the outward-facing states). The transition, $C_{1a} \rightarrow C_1$ is clearly related to the slow component of the experimental transient currents. At depolarizing potential (+70 mV), the starting probabilities for WT and Q457C-MTSET are similar (C_6 is ~80% and C_{1a} is ~20%; Fig. 8, A and C) and different with the starting probabilities for Q457C (C_6 is ~70% and C_{1a} is ~30%; Fig. 8 B). At hyperpolarizing potential (−150 mV), the rate of Q457C-MTSET to pass through the slow transition (C_{1a}; Fig. 8 E) and reach the outward-facing state (C_2; Fig. 8 D), is faster than those of

WT and Q457C. The occupancy probability for WT, Q457C and Q457C-MTSET is consistent with the experimental slow decay constants.

Fig. 9 shows the variability of the occupancy probabilities (C_i) in 100 mM Na$^+$ with voltage. The occupancy probabilities of predominant state (C_2) at the extreme negative voltage (−150 mV) are 97%, 97% and 94% for WT, Q457C and Q457C-MTSET of rSGLT1, respectively. The occupancy probabilities of predominant state (C_6) at the extreme positive voltage (+70 mV) are 76%, 68% and 79% for WT, Q457C and Q457C-MTSET of rSGLT1, respectively. For WT rSGLT1, the occupancy probabilities of C_2, C_1, C_{1a}, and C_6 at −50 mV based on the decay constants in Table 3 are 26%, 10%, 43% and 21%, suggesting that 36% of transporters are in an outward-facing free or Na$^+$-bound state. However, based on a five-state kinetic model, the occupancy probabilities of WT hSGLT1 in a free or Na$^+$-bound state at −50 mV are 73% (23,26,33). The discrepancy between these two sets of observations is due to the different values of V$_{1/2}$ for WT hSGLT1 (−46 ± 3 mV) (33) and WT rSGLT1 (−2.5 ± 0.7 mV) (6). For mutant Q457C rSGLT1, the occupancy probabilities of C_2, C_1, C_{1a}, and C_6 at −50 mV are 26%, 34%, 23% and 17%, suggesting that 60% of transporters are in a free or Na$^+$-bound state. For mutant Q457C rSGLT1 exposed to MTSET, the occupancy probabilities of C_2, C_1, C_{1a}, and C_6 at −50 mV are 28%, 43%, 20% and 9%, suggesting that 71% of transporters are in a free or Na$^+$-bound state. The occupancy probability for WT, Q457C, and Q457C-MTSET is consistent with the hypothesis that Q457C-MTSET is preferentially occupies an outward–facing state.

Gagnon et al. (33) found a disulfide bridge between C255 and C511 of hSGLT1, and were first to quantitatively study the dose-dependent effect of αMG on the pre-steady-state
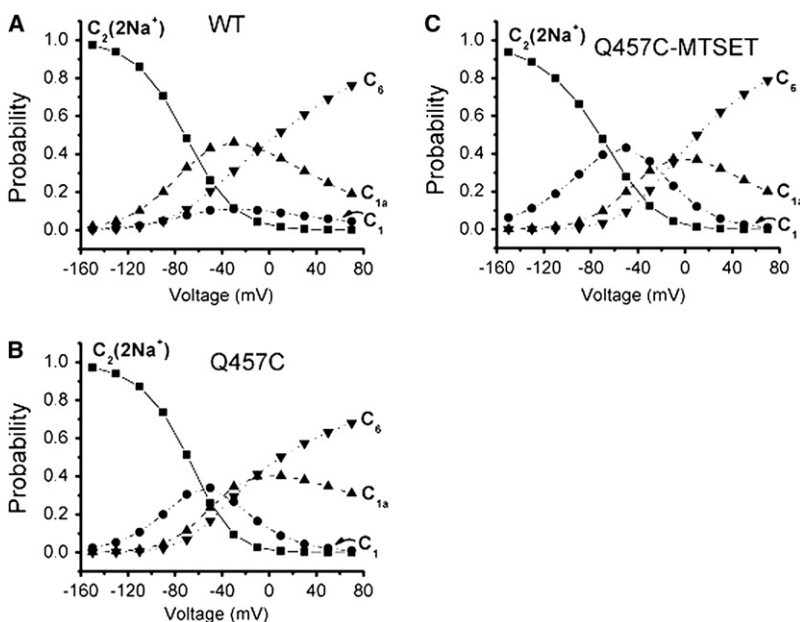

FIGURE 9 Simulation predictions on occupancy probabilities (C_i) in 100 mM Na$^+$ as a function of voltage as calculated by the four-state kinetic model for WT rSGLT1 (A), mutant Q457C (B), and Q457C exposed to MTSET (C).

currents of these mutants as well as for WT hSGLT1 (23). They also proposed a five-state kinetic model to quantitatively explain the effect of αMG on the pre-steady-state currents. They found that the reorientation of free transporter was the slowest step for WT hSGLT1 either in the presence or in the absence of αMG.

In this study, we suggest that modulation of charge and polarity of glutamine 457 in rSGLT1 likely influences sugar translocation by affecting reorientation of the empty carrier from one side of the membrane to the other side. Because no steady-state currents could be measured for mutants Q457C-MTSET and Q457R of rSGLT1, we could not study the mutants' effect on reorientation of the fully loaded carrier from one side of the membrane to the other side.

Since our results show an outward-facing preference of the empty carrier, together with the findings from Gagnon et al. (23), it seems reasonable to speculate that modulation of charge and polarity of glutamine 457 likely influences sugar translocation by affecting reorientation of the fully loaded carrier from one side of the membrane to the other side.

In summary, the experimental and computer simulation data may provide a better understanding of the relationships for charge/conformational change and translocation at the position 457 in rSGLT1. As an explanation for the altered conformational equilibrium, it is possible that mutants Q457C-MTSET and Q457R may disrupt the intramolecular interactions involved in stabilizing the transporter in the inward facing conformation and that this results in an impaired ability of the transporter to return to this conformation. Therefore, the transporter may accumulate in the outward facing conformation. Taken together, in addition to its involvement in sugar binding (13,14), our results suggest that modulation of charge and polarity of glutamine 457 in rSGLT1 is likely associated with a minor modification of the orientation of the free carrier and a complete abolition of the translocation of the fully loaded carrier.

REFERENCES

1. Martin, M. G., E. Turk, M. P. Lostao, C. Kerner, and E. M. Wright. 1996. Defects in Na+/glucose cotransporter (SGLT1) trafficking and function cause glucose-galactose malabsorption. *Nat. Genet.* 12:216–220.

2. Balen, D., M. Ljubojevic, D. Breljak, H. Brzica, V. Zlender, et al. 2008. Revised immunolocalization of the Na+-D-glucose cotransporter SGLT1 in rat organs with an improved antibody. *Am. J. Physiol. Cell Physiol.* C475–C489.

3. Hirsh, A. J., and C. I. Cheeseman. 1998. Cholecystokinin decreases intestinal hexose absorption by a parallel reduction in SGLT1 abundance in the brush-border membrane. *J. Biol. Chem.* 273:14545–14549.

4. Althoff, T., H. Hentschel, J. Luig, H. Schutz, M. Kasch, et al. 2007. Na+-D-glucose cotransporter in the kidney of Leucoraja erinacea: molecular identification and intrarenal distribution. *Am. J. Physiol. Regul. Integr. Comp. Physiol.* 292:R2391–2399.

5. Turk, E., and E. M. Wright. 1997. Membrane topology motifs in the SGLT cotransporter family. *J. Membr. Biol.* 159:1–20.

6. Lo, B., and M. Silverman. 1998. Cysteine scanning mutagenesis of the segment between putative transmembrane helices IV and V of the high affinity Na+/Glucose cotransporter SGLT1. Evidence that this region participates in the Na+ and voltage dependence of the transporter. *J. Biol. Chem.* 273:29341–29351.

7. Loo, D. D., B. A. Hirayama, E. M. Gallardo, J. T. Lam, E. Turk, et al. 1998. Conformational changes couple Na+ and glucose transport. *Proc. Natl. Acad. Sci. USA.* 95:7789–7794.

8. Tyagi, N. K., A. Kumar, P. Goyal, D. Pandey, W. Siess, et al. 2007. D-Glucose-recognition and phlorizin-binding sites in human sodium/D-glucose cotransporter 1 (hSGLT1): a tryptophan scanning study. *Biochemistry.* 46:13616–13628.

9. Gagnon, D. G., C. Frindel, and J. Y. Lapointe. 2007. Voltage-clamp fluorometry in the local environment of the C255–C511 disulfide bridge of the Na+/glucose cotransporter. *Biophys. J.* 92:2403–2411.

10. Puntheeranurak, T., M. Kasch, X. Xia, P. Hinterdorfer, and R. K. Kinne. 2007. Three surface subdomains form the vestibule of the Na+/glucose cotransporter SGLT1. *J. Biol. Chem.* 282:25222–25230.

11. Loo, D. D., B. A. Hirayama, A. Cha, F. Bezanilla, and E. M. Wright. 2005. Perturbation analysis of the voltage-sensitive conformational changes of the Na+/glucose cotransporter. *J. Gen. Physiol.* 125:13–36.

12. Meinild, A. K., B. A. Hirayama, E. M. Wright, and D. D. Loo. 2002. Fluorescence studies of ligand-induced conformational changes of the Na(+)/glucose cotransporter. *Biochemistry.* 41:1250–1258.

13. Diez-Sampedro, A., E. M. Wright, and B. A. Hirayama. 2001. Residue 457 controls sugar binding and transport in the Na(+)/glucose cotransporter. *J. Biol. Chem.* 276:49188–49194.

14. Hirayama, B. A., D. D. Loo, A. Diez-Sampedro, D. W. Leung, A. K. Meinild, et al. 2007. Sodium-dependent reorganization of the sugar-binding site of SGLT1. *Biochemistry.* 46:13391–13406.

15. Panayotova-Heiermann, M., S. Eskandari, E. Turk, G. A. Zampighi, and E. M. Wright. 1997. Five transmembrane helices form the sugar pathway through the Na+/glucose cotransporter. *J. Biol. Chem.* 272:20324–20327.

16. Huntley, S. A., D. Krofchick, and M. Silverman. 2004. Position 170 of rabbit Na+/glucose cotransporter (rSGLT1) lies in the Na+ pathway; modulation of polarity/charge at this site regulates charge transfer and carrier turnover. *Biophys. J.* 87:295–310.

17. Lo, B., and M. Silverman. 1998. Replacement of Ala-166 with cysteine in the high affinity rabbit sodium/glucose transporter alters transport kinetics and allows methanethiosulfonate ethylamine to inhibit transporter function. *J. Biol. Chem.* 273:903–909.

18. Chen, X. Z., M. J. Coady, F. Jalal, B. Wallendorff, and J. Y. Lapointe. 1997. Sodium leak pathway and substrate binding order in the Na+-glucose cotransporter. *Biophys. J.* 73:2503–2510.

19. Parent, L., S. Supplisson, D. D. Loo, and E. M. Wright. 1992. Electrogenic properties of the cloned Na+/glucose cotransporter: I. Voltage-clamp studies. *J. Membr. Biol.* 125:49–62.

20. Liu, T., B. Lo, P. Speight, and M. Silverman. 2008. Transmembrane IV of the high-affinity sodium-glucose cotransporter participates in sugar binding. *Am. J. Physiol. Cell Physiol.* 295:C64–C72.

21. Krofchick, D., and M. Silverman. 2003. Investigating the conformational States of the rabbit na(+)/glucose cotransporter. *Biophys. J.* 84:3690–3702.

22. Huntley, S. A., D. Krofchick, and M. Silverman. 2006. A glutamine to glutamate mutation at position 170 (Q170E) in the rabbit Na+/glucose cotransporter, rSGLT1, enhances binding affinity for Na+. *Biochemistry.* 45:4653–4663.

23. Gagnon, D. G., C. Frindel, and J. Y. Lapointe. 2007. Effect of substrate on the pre-steady-state kinetics of the Na+/glucose cotransporter. *Biophys. J.* 92:461–472.

24. Loo, D. D., B. A. Hirayama, M. H. Karakossian, A. K. Meinild, and E. M. Wright. 2006. Conformational dynamics of hSGLT1 during Na+/glucose cotransport. *J. Gen. Physiol.* 128:701–720.

25. Hirayama, B. A., A. Diez-Sampedro, and E. M. Wright. 2001. Common mechanisms of inhibition for the Na+/glucose (hSGLT1) and Na+/Cl-/GABA (hGAT1) cotransporters. *Br. J. Pharmacol.* 134:484–495.

26. Chen, X. Z., M. J. Coady, and J. Y. Lapointe. 1996. Fast voltage clamp discloses a new component of presteady-state currents from the Na(+)-glucose cotransporter. *Biophys. J.* 71:2544–2552.

27. Loo, D. D., A. Hazama, S. Supplisson, E. Turk, and E. M. Wright. 1993. Relaxation kinetics of the Na+/glucose cotransporter. *Proc. Natl. Acad. Sci. USA.* 90:5767–5771.

28. Panayotova-Heiermann, M., D. D. Loo, M. P. Lostao, and E. M. Wright. 1994. Sodium/D-glucose cotransporter charge movements involve polar residues. *J. Biol. Chem.* 269:21016–21020.

29. Loland, C. J., C. Granas, J. A. Javitch, and U. Gether. 2004. Identification of intracellular residues in the dopamine transporter critical for regulation of transporter conformation and cocaine binding. *J. Biol. Chem.* 279:3228–3238.

30. MacAulay, N., A. K. Meinild, T. Zeuthen, and U. Gether. 2003. Residues in the extracellular loop 4 are critical for maintaining the conformational equilibrium of the gamma-aminobutyric acid transporter-1. *J. Biol. Chem.* 278:28771–28777.

31. Pinkett, H. W., A. T. Lee, P. Lum, K. P. Locher, and D. C. Rees. 2007. An inward-facing conformation of a putative metal-chelate-type ABC transporter. *Science.* 315:373–377.

32. Abramson, J., I. Smirnova, V. Kasho, G. Verner, H. R. Kaback, et al. 2003. Structure and mechanism of the lactose permease of Escherichia coli. *Science.* 301:610–615.

33. Gagnon, D. G., P. Bissonnette, and J. Y. Lapointe. 2006. Identification of a disulfide bridge linking the fourth and the seventh extracellular-loops of the na+/glucose cotransporter. *J. Gen. Physiol.* 127:145–158.

34. Parent, L., S. Supplisson, D. D. Loo, and E. M. Wright. 1992. Electrogenic properties of the cloned Na+/glucose cotransporter: II. A transport model under nonrapid equilibrium conditions. *J. Membr. Biol.* 125:63–79.